Characterization of structural uncertainty in LES of a round jet

By L. Jofre, S. P. Domino† AND G. Iaccarino

1. Motivation and objectives

Large-eddy simulation (LES) has become a high-fidelity reference approach for the study of a broad range of complex turbulent flows. Some examples include multiphase flows (Kuerten 2016), geophysical fluid dynamics (Smagorinsky 1963), and turbulent combustion (Pitsch 2006). Compared with direct numerical simulation (DNS), LES reduces the computational cost of solving turbulent flows by applying a low-pass filter to the conservation equations. For example, the number of grid points N required in LES of free shear layers scales with the Reynolds number as $N^3 \sim Re$ (Pope 2000), while resolving all the turbulent flow motions entails performing DNS of the order $N^3 \sim Re^{9/4}$. The reduction in computational cost, however, is obtained at expenses of modeling the effects of the small scales on the resolved flow field in terms of subfilter stresses. Consequently, the assumptions introduced in the closure formulations become potential sources of model-form uncertainty that can affect the quantities of interest (QoI).

Numerous studies have been dedicated to identify sources of error resulting from the numerical approximations required to discretely solve the LES conservation equations. Some of the most notable works are the seminal paper by Ghosal (1996) and the detailed error database gathered by Meyers *et al.* (2003). However, even with the widespread utilization of LES in many scientific and technological fields, few studies have analyzed model-form incertitude from an uncertainty quantification (UQ) point of view. In general, most analyses are based on nonintrusive methodologies applied to simple flow configurations and are concerned mainly with sensitivities to LES closure parameters, such as model coefficients (Meldi *et al.* 2011), filter characteristics (Meyers & Sagaut 2007*a*) or mesh resolution (Meyers & Sagaut 2007*b*). A more sophisticated approach is to consider the closure parameters uncertain and estimate their effects on the QoIs by forward-propagating them as probability distributions. This strategy has been applied to Reynolds-averaged Navier-Stokes (RANS) (Dunn *et al.* 2011) and LES (Lucor *et al.* 2007) models and extended to incorporate simulation data from DNS (Völker *et al.* 2002) and utilize Bayesian inference techniques (Cheung *et al.* 2011; Safta *et al.* 2017). In the case of complex flows, some methodologies predict on the basis of an ensemble of solutions obtained using different models, such as in earth sciences for weather and ocean forecasting (Phillips 1970; Stevens *et al.* 2005). Although common practice, all these approaches present important impediments to generalization owing to their dependency on the underlying structure of the models utilized. In this regard, the present work aims to analyze sensitivity to model-form uncertainty in LES of an axisymmetric turbulent jet following a systematic strategy recently presented in Jofre *et al.* (2018). The framework developed is inspired by an approach previously introduced in RANS modeling (Gorlé & Iaccarino 2013; Emory *et al.* 2013; Iaccarino *et al.* 2017). However, its extension to LES

† Computational Thermal and Fluid Mechanics, Sandia National Laboratories

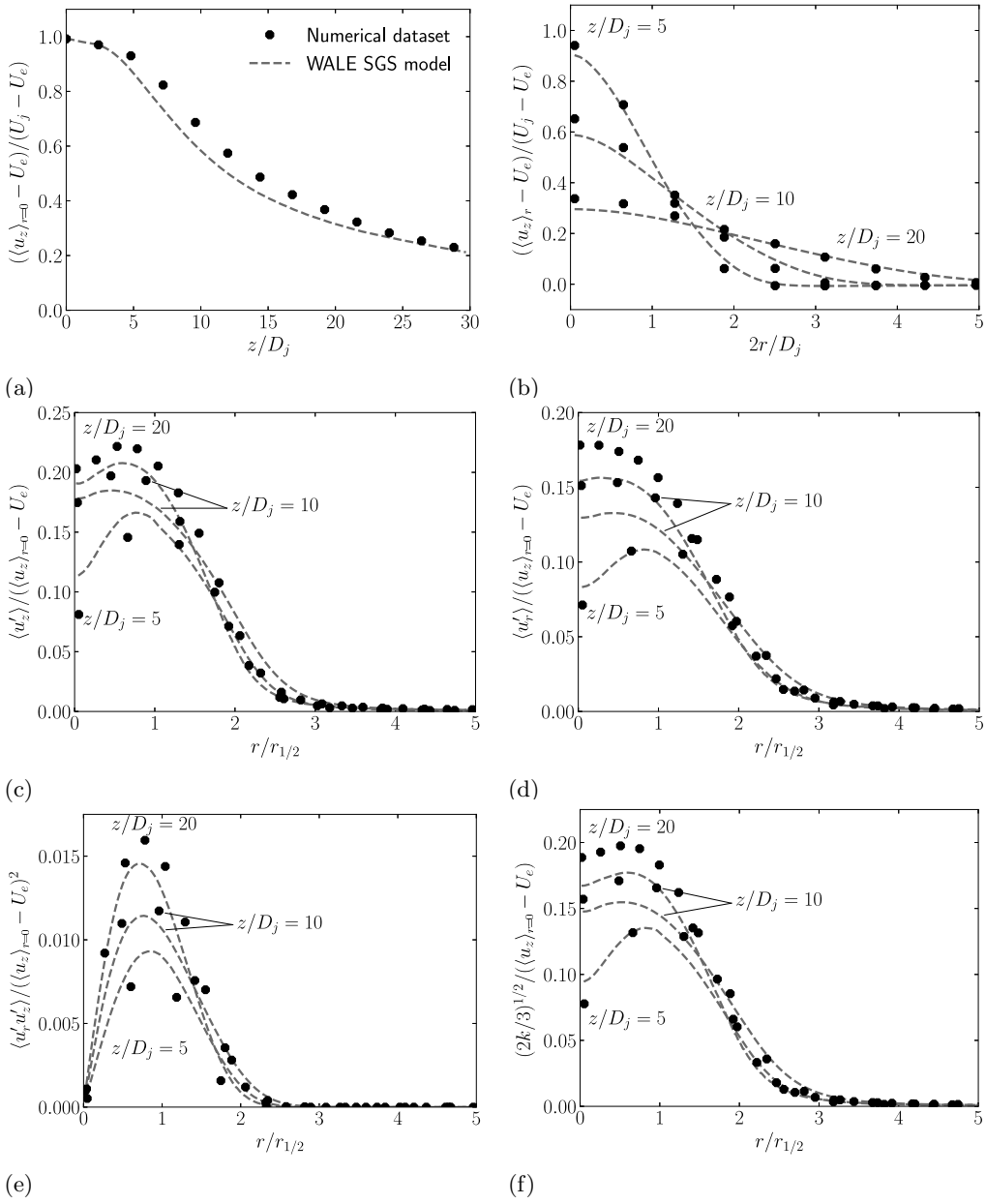

FIGURE 1. Comparison of WALE SGS model results against the numerical dataset. (a) Mean axial velocity along the jet axis. (b) Radial profiles of mean axial velocity at several axial positions. (c) Radial profiles of rms axial velocity at different axial positions. (d) Radial profiles of rms radial velocity at different axial positions. (e) Radial profiles of Reynolds shear stress at different axial positions. (f) Radial profiles of turbulent kinetic energy at different axial positions.

required revisiting the underlying assumptions, mathematical derivation and physical bounds of the methodology. In short, the approach is based on introducing perturbations to the decomposed, small-scale stress tensor within a range of physically plausible values. These perturbations correspond to discrepancy in magnitude (trace), shape (eigenvalues)

$C\left(\bar{\tau}_{ij}, \tau_{ij}^{SGS}\right)$	$r/r_{1/2} \approx 0$	$r/r_{1/2} \approx 1$	$r/r_{1/2} \approx 2$
$z/D_j \approx 1$	0.34	0.38	0.68
$z/D_j \approx 5$	0.37	0.56	0.71
$z/D_j \approx 20$	0.43	0.64	0.73

TABLE 1. Correlation coefficient between $\bar{\tau}_{ij}$ and τ_{ij}^{SGS} at different axial and radial positions.

and orientation (eigenvectors) of the normalized, small-scale stresses with respect to a given tensor state. The generality of the framework with respect to the six degrees of freedom of the small-scale stress tensor also makes it suitable for its application within data-driven techniques, such as the approaches recently developed to improve RANS predictions (Parish & Duraisamy 2016; Xiao *et al.* 2016).

The axisymmetric, or circular, jet is a canonical fluid flow found in many scientific and industrial problems. Jets are common in the natural world, for instance, in volcano eruptions, in motion and defense mechanisms of animals, in water and steam discharge of geysers, or in convective thermals in cloud physics, as well as in industrial applications involving mixing, heating and cooling, and propulsion, such as fuel injection in combustors, cooling of turbine blades, propulsion of high-speed vessels, inkjet printers, or boundary layer flow separation control. Most LES calculations of circular turbulent jets are based on eddy-viscosity-type models or dissipative numerical schemes (e.g., Olsson & Fuchs (1996), Wang *et al.* (2008), Kim & Choi (2009)). The general observation in such studies is that first-order flow quantities in the axial and radial directions are well predicted, as these depend mostly on large-scale motions, whereas higher-order statistics, viz. velocity fluctuations and shear stresses, are typically not well represented. Therefore, this work systematically analyzes the impact of subfilter modeling assumptions on the QoIs to characterize underlying *a-priori* and *a-posteriori* differences of LES closure models.

A complete description of the UQ framework can be found in Jofre *et al.* (2018). Therefore, the paper is organized as follows. First, a comprehensive description of the jet's reference dataset generated for this work is described in Section 2. Next, in Section 3, discrepancies between reference and base LES results are analyzed. The observations are subsequently related to sensitivity in subgrid-scale (SGS) stress model-form uncertainty in Section 4. Finally, conclusions are drawn and future work is discussed in Section 5.

2. Description of the numerical reference dataset

The flow studied is based on the circular jet experimentally studied by Amielh *et al.* (1996). The experimental data are utilized to validate the numerical dataset generated in this work. Numerical results of the flow are obtained by means of the unstructured and massively parallel low-Mach-number flow solver Nalu (Domino 2015).

The flow corresponds to an axisymmetric turbulent jet at $Re = U_j D_j/\nu = 21000$ based on the axial velocity at the jet exit, $U_j = 12$ m/s, the jet nozzle diameter, $D_j = 2.6 \cdot 10^{-2}$ m, and the kinematic viscosity of the fluid, ν. The jet discharges from a long pipe (modeled with periodic boundaries) into a slow coflow, $U_e = 9{\cdot}10^{-1}$ m/s, of the same fluid. Subscripts j and e correspond to the jet flow and external coflow, respectively. The

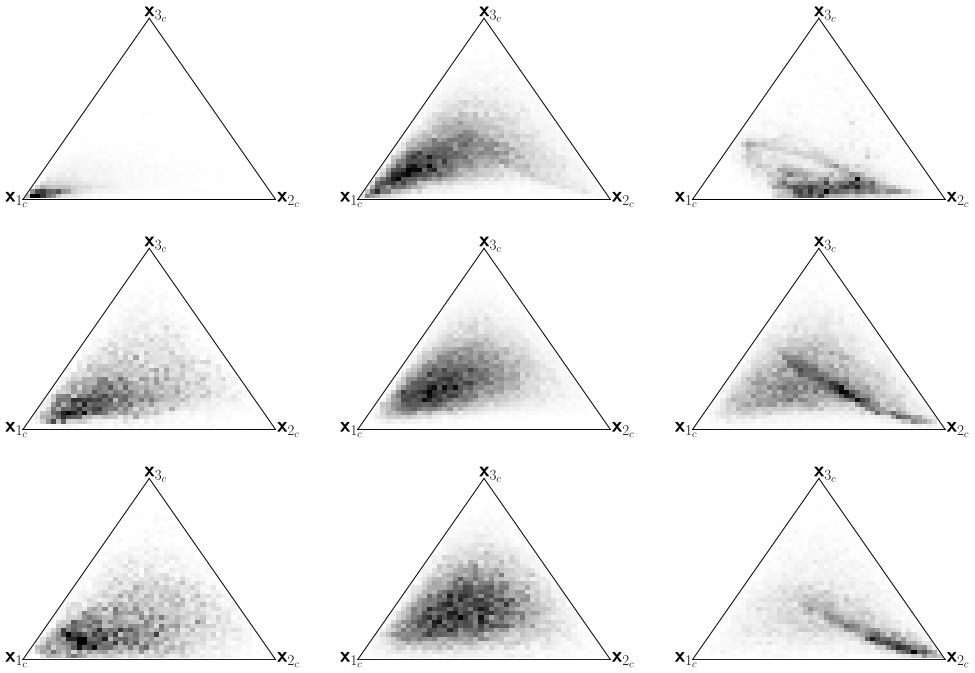

FIGURE 2. PDF of $\overline{\tau}_{ij}$ anisotropy represented on the barycentric map at different axial and radial positions. Rows: (top) $z/D_j \approx 1$, (center) $z/D_j \approx 5$, (bottom) $z/D_j \approx 20$. Columns: (left) $r/r_{1/2} \approx 0$, (center) $r/r_{1/2} \approx 1$, (right) $r/r_{1/2} \approx 2$.

ratios between pipe diameter and computational domain are $D_e/D_j = 20$ and $L/D_j = 30$. The inlet jet velocity is extracted from a plane perpendicular to the axis of a periodic turbulent pipe flow with momentum flux $M_j = 1 \cdot 10^{-1}$ N, a uniform velocity profile is utilized for the co-flow, and specified-pressure open boundary conditions are imposed at the exit and lateral surfaces of the domain. All simulations start from the jet discharging into a fluid with initial velocity U_e. The averaging is started once a sufficiently long transient period is surpassed, $t\,U_j/L \approx 10$, and statistics are collected over a time period of $\Delta t\,U_j/D_j \approx 1000$. Additional averaging is performed in the azimuthal direction.

The mesh designed to carefully perform high-fidelity simulations of the flow (DNS-like resolution) is based on scaling arguments for free shear flows (Cantwell 2002). The timescale of the large eddies in a turbulent jet can be estimated as $t_l \sim D_j/U_j$. If it is assumed that the kinetic energy supply rate is proportional to the inverse of this timescale, the dissipation rate can be approximated by $\epsilon \sim U_j^3/D_j$. As a result, the Kolmogorov length scale can be estimated as $\eta \equiv \left(\nu^3/\epsilon\right)^{1/4} \sim D_j/Re^{3/4}$. Following this scaling, the computational domain is spatially discretized by means of an axisymmetric mesh of approximately 200M control volumes with resolutions of $\Delta/\eta \sim \mathcal{O}(1)$.

3. Discrepancy between reference and LES results

The first step is to characterize discrepancies between τ_{ij} evaluated from filtering the numerical dataset to directly calculate $\bar{\tau}_{ij}$, and the second step is to evaluate τ_{ij}^{SGS} based on the Wall-Adapting Local Eddy-Viscosity (WALE) SGS model (Nicoud & Ducros

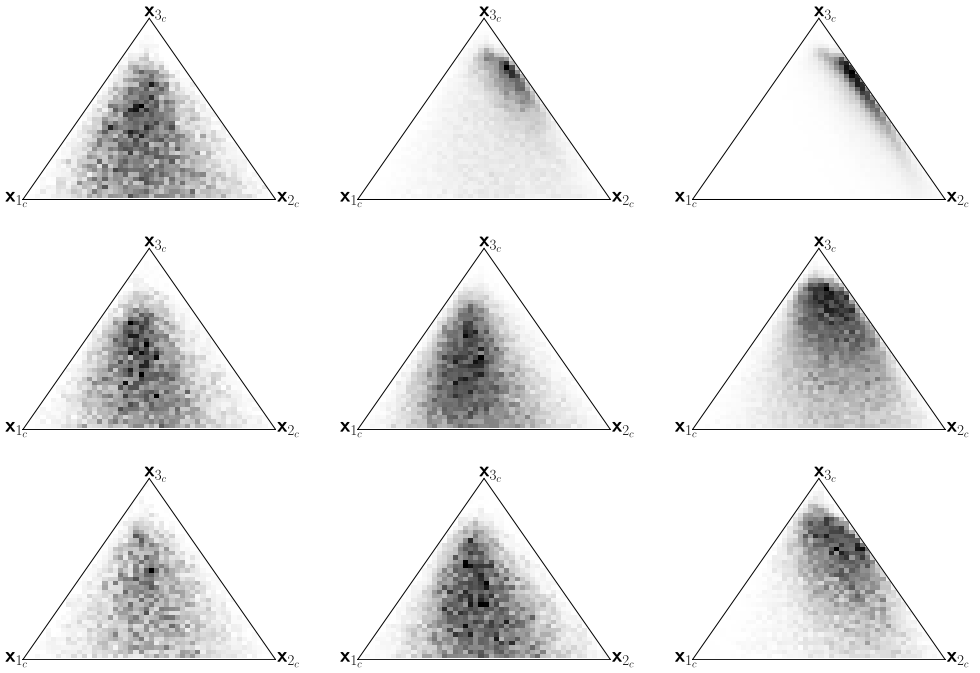

FIGURE 3. PDF of WALE τ_{ij}^{SGS} anisotropy represented on the barycentric map at different axial and radial positions. Rows: (top) $z/D_j \approx 1$, (center) $z/D_j \approx 5$, (bottom) $z/D_j \approx 20$. Columns: (left) $r/r_{1/2} \approx 0$, (center) $r/r_{1/2} \approx 1$, (right) $r/r_{1/2} \approx 2$.

1999). The $\bar{\tau}_{ij} = \overline{u_i u_j} - \overline{u}_i \overline{u}_j$ data are obtained by filtering five instantaneous velocity snapshots at different flow through times (FFT), defined as FFT $\sim L/U_j$, of the dataset described in Section 2. The filtering operation is carried out by means of a second-order Gaussian filter (Sagaut & Grohens 1999)

$$\overline{\phi} = \phi + \frac{\bar{\Delta}^2}{24} \frac{\partial^2 \phi}{\partial x_i^2} + \mathcal{O}(\bar{\Delta}^4). \tag{3.1}$$

Data for the WALE-SGS-modeled $\tau_{ij}^{SGS} = -2\nu_{SGS}\overline{S}_{ij} + \tau_{kk}^{SGS}\delta_{ij}/3$ are computed from the filtered snapshots (i) by utilizing the definition of the model and (ii) by performing LES on the computational setup described in Section 2 on a mesh of approximately 3M control volumes with a resolution of $\Delta/\eta \sim 5$. Similar to the filtered case, five instantaneous velocity field snapshots at different FTTs are utilized for the analysis. The filter width in Eq. (3.1) is set to an equivalent LES mesh resolution of $\bar{\Delta}/\eta \sim 5$.

3.1. *Comparison of LES against the numerical reference dataset*

Prior to presenting the differences between filtered and modeled tensors from reference data, Figure 1 summarizes the accuracy of the LES compared with that of the DNS-like numerical dataset in terms of first- and second-order statistics. The extension of the potential core and axisymmetric decay in the interaction region is underpredicted as shown by the mean axial velocity along the jet axis ($2 < z/D_j < 22$) and the corresponding radial profiles (Figure 1(a,b)). This underprediction is connected to large stresses near the jet nozzle ($z/D_j \leq 5$) indicative of a rapid development of the shear layer (Figure 1(c,d,e,f)) as a result of flow instabilities growing too fast. Far downstream in the

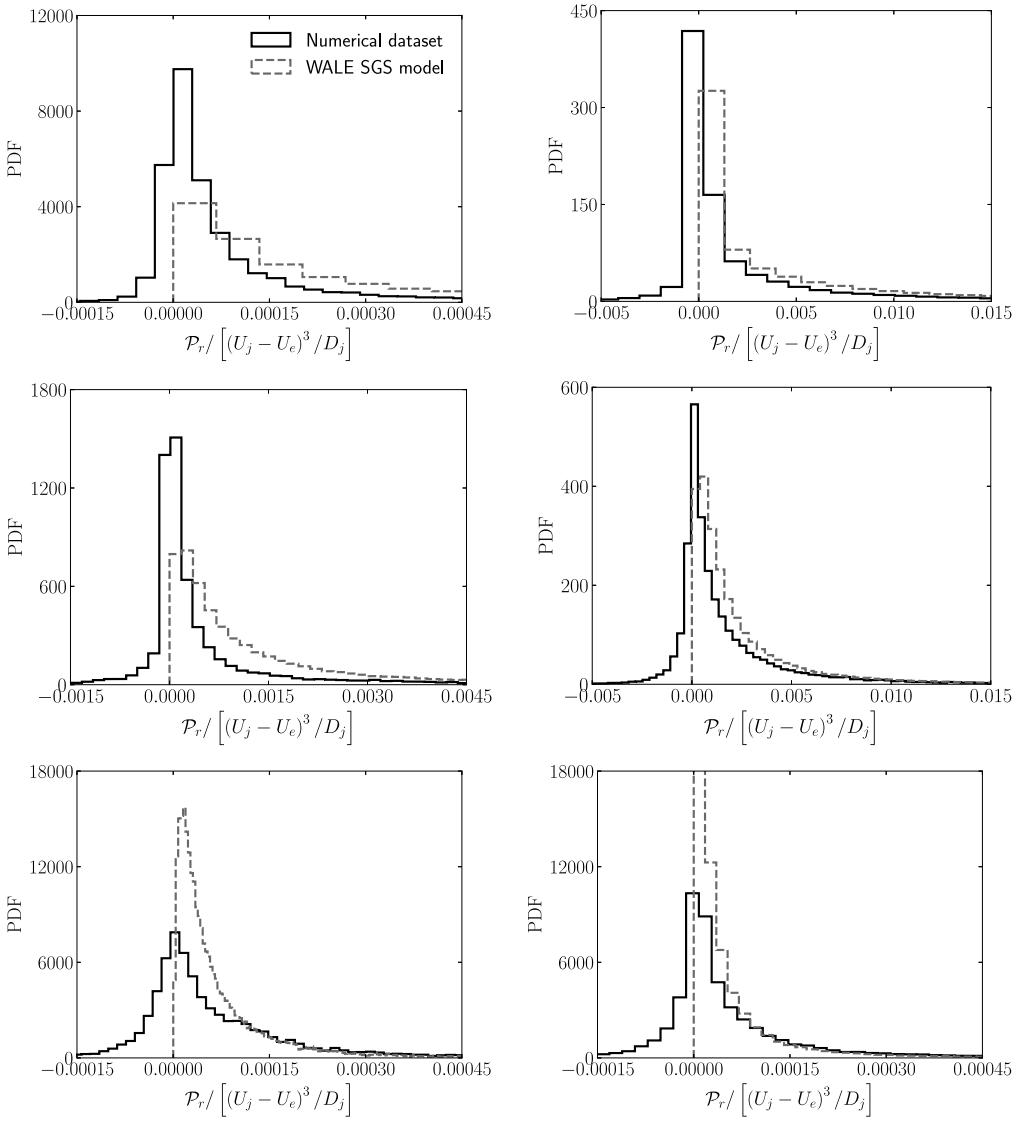

FIGURE 4. PDF of filtered and modeled $\mathcal{P}_r$ normalized by $(U_j - U_e)^3 / D_j$ at different axial and radial positions. Rows: (top) $z/D_j \approx 1$, (center) $z/D_j \approx 5$, (bottom) $z/D_j \approx 20$. Columns: (left) $r/r_{1/2} \approx 0$, (right) $r/r_{1/2} \approx 1$.

fully developed region ($z/D_j > 25$), where turbulent mixing prevails, the axial velocity recovers to match the reference data, while the shear stresses become underestimated owing to the prematurely development of the shear layer. The flow in the outer layer region, which is dominated by large-scale entrainment motions, is well predicted as shown by the radial profiles above $r/r_{1/2} \approx 1$ collapsing with the reference dataset. The normal stresses, and their aggregate representation through the turbulent kinetic energy, follow the same trend as the mean and shear stress statistics, viz. overprediction near the jet nozzle ($z/D_j \leq 5$) and underestimation in the developed flow region ($z/D_j \geq 10$) for

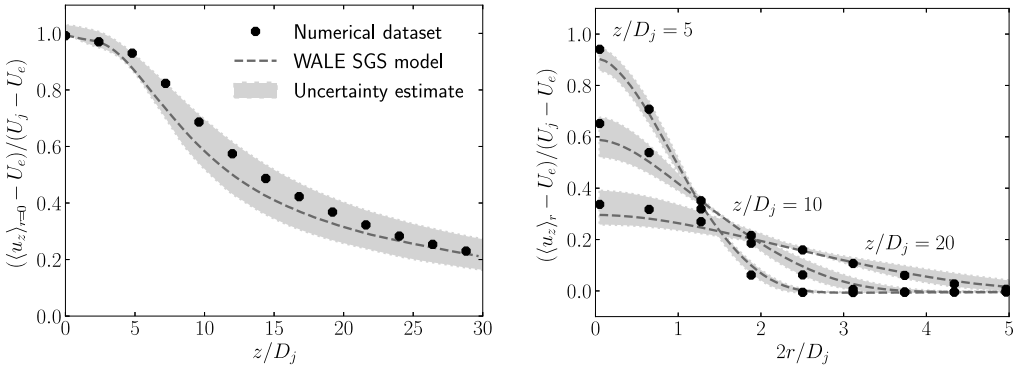

(a) (b)

FIGURE 5. Comparison of WALE SGS uncertainty estimates against the numerical dataset. (a) Mean axial velocity along the jet axis. (b) Radial profiles of mean axial velocity at several axial positions.

$r/r_{1/2} < 2$, whereas significantly good agreement with the reference results for the outer layer region is shown.

3.2. *Correlation coefficient discrepancy*

The conventional procedure to analyze discrepancy between filtered and modeled τ_{ij} is to calculate the correlation coefficient between the two tensors by means of the normalized inner product (Clark *et al.* 1979)

$$C\left(\bar{\tau}_{ij}, \tau_{ij}^{SGS}\right) = \langle \bar{\tau}_{ij} \tau_{ij}^{SGS} \rangle / \left(\langle \bar{\tau}_{ij} \bar{\tau}_{ij} \rangle^{1/2} \langle \tau_{ij}^{SGS} \tau_{ij}^{SGS} \rangle^{1/2} \right), \tag{3.2}$$

which is $C = 1$ for perfectly correlated tensors and $C = 0$ otherwise. The correlation coefficients at axial positions $z/D_j \approx 1, 5, 20$ and radial distances $r/r_{1/2} \approx 0, 1, 2$ are listed in Table 1. In general, correlation improves downstream in the axial direction as turbulent mixing becomes more dominant. For a given axial position, the model performs best in the outer layer followed by the shear layer and worst in the centerline. The correlation coefficient provides a quantitative measure of the performance of the model. However, this measurement is very broad as it does not detail the rationale of the underlying differences.

3.3. *Eigenspace-based discrepancy*

The tensor eigendecompostion offers a complimentary approach to the correlation coefficient. The discrepancy measurement is less compact since it does not provide a single scalar value, but it is potentially more informative as it allows one to separately analyze the differences in terms of magnitude, shape and orientation. This methodology is utilized next to further characterize the differences between $\bar{\tau}_{ij}$ and τ_{ij}^{SGS}.

Focus is placed on the difference in anisotropy on the basis of the PDFs shown on the barycentric map (Banerjee *et al.* 2007) for $\bar{\tau}_{ij}$ and τ_{ij}^{SGS} in Figures 2 and 3, respectively. From the $\bar{\tau}_{ij}$ perspective, the anisotropy of τ_{ij} in the centerline region remarkably evolves from the purely one-component limit at $z/D_j \approx 1$ to a wide PDF between axisymmetric expansion and the two-component limit at $z/D_j \approx 5, 10$; the initial one-component shape is imposed by the walls of the pipe from which the jet discharges. This trend is similarly observed for $r/r_{1/2} \approx 1$, but less accentuated as the distribution at $z/D_j \approx 1$ is more

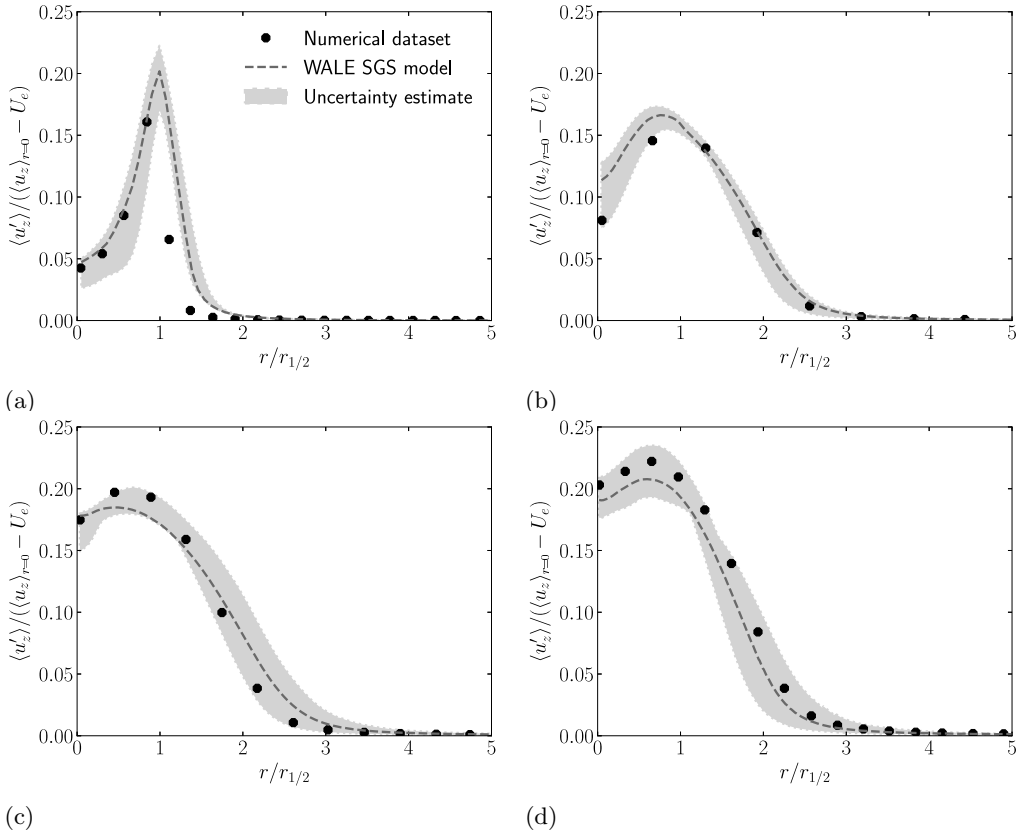

FIGURE 6. Comparison of WALE SGS uncertainty estimates against the numerical dataset. Radial profiles of rms axial velocity at different axial positions: (a) $z/D_j \approx 1$, (b) $z/D_j \approx 5$, (c) $z/D_j \approx 10$, (d) $z/D_j \approx 20$.

stretched. A completely different behavior is depicted for $r/r_{1/2} \approx 2$. The mode of the PDF is initially located along the central region of the two-component limit, and with increasing z/D_j it shifts toward a narrow distribution starting at the two-component vertex and following approximately the line of plane strain. The picture for τ_{ij}^{SGS} is notably different. At the centerline region, the shape of τ_{ij}^{SGS} is spread over the central and bottom regions of the barycentric map and it does not differ substantially between axial locations. The same anisotropy distribution is revealed for $r/r_{1/2} \approx 1$ at $z/D_j \approx 5, 20$. For the remaining locations, the mode of the PDFs is found at the axisymmetric contraction limit close to the three-component vertex. The distributions are narrow and stretched along the axisymmetric contraction limit for $z/D_j \approx 1$, whereas they spread toward the central region for $z/D_j \approx 5, 20$.

3.4. *Production of SGS kinetic energy discrepancy*

The anisotropy and orientation imposed on τ_{ij}^{SGS} in eddy-viscosity-type models force $\mathcal{P}_r$ to act as a sink of filtered kinetic energy. The dynamic approach (Germano *et al.* 1991) relaxes this constraint by allowing ν_{SGS} to take negative values in particular regions of the flow on the basis of the Germano identity (Germano 1992) and a test-filtering operation. This methodology enables $\mathcal{P}_r$ to take negative values locally, and therefore it relatively

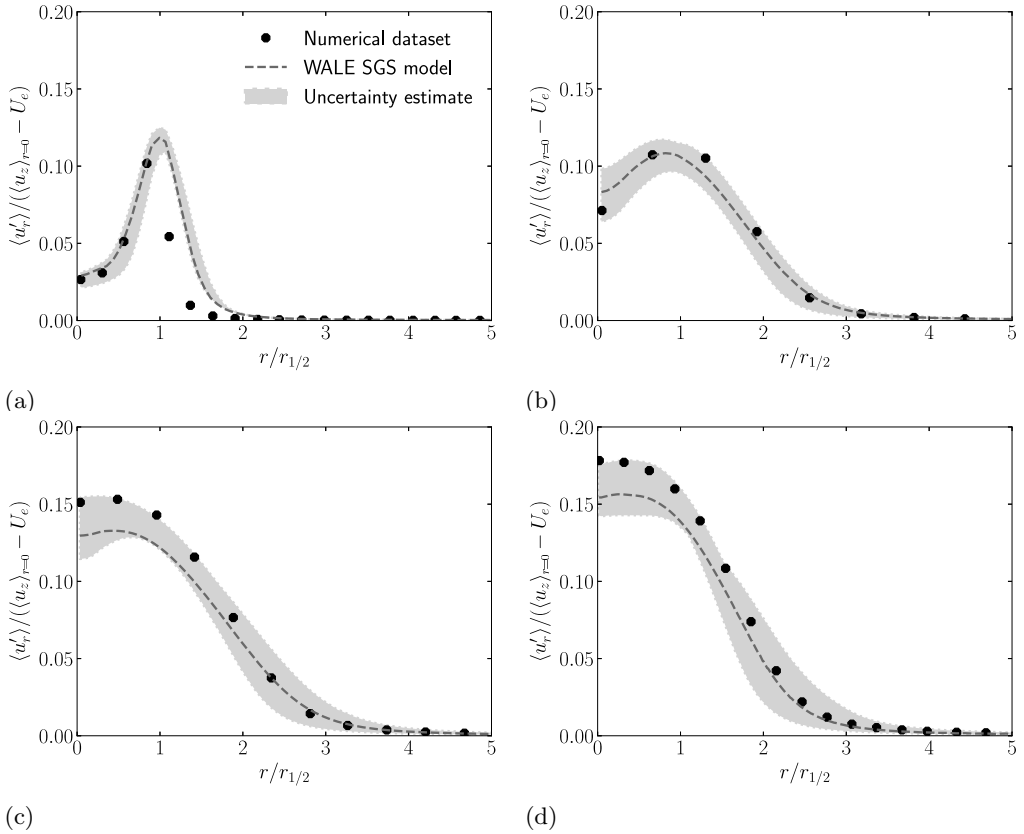

FIGURE 7. Comparison of WALE SGS uncertainty estimates against the numerical dataset. Radial profiles of rms radial velocity at different axial positions: (a) $z/D_j \approx 1$, (b) $z/D_j \approx 5$, (c) $z/D_j \approx 10$, (d) $z/D_j \approx 20$.

accounts for backscatter effects. In terms of kinetic energy transport the negative sign of ν_{SGS} can be directly interpreted from an eigenspace perspective as a permutation between the first and third eigenvectors of the SGS stress tensor; namely, τ_{ij}^{SGS} and $\overline{S}_{ij}$ share the same eigenvalues and are rotated with respect to the first and third principal directions. In the case of utilizing the WALE SGS model, ν_{SGS} is dynamically calculated on the basis of the invariants of the velocity gradient tensor (recovering, for example, cubic behavior at walls (Chapman & Kuhn 1986)), however, defined always nonnegative by construction.

The discrepancy between normalized reference and modeled $\mathcal{P}_r / \left[(U_j - U_e)^3 / D_j \right]$ at different axial and radial positions is depicted in Figure 4. An important observation is that the filtered numerical dataset exhibits significant amounts of backscatter (points of the PDF with $\mathcal{P}_r < 0$). This effect is not completely captured by the modeled $\mathcal{P}_r$ because of the aforementioned limitations of eddy-viscosity-type models as shown by the nonnegative distributions. In general, the mean of $\mathcal{P}_r$ is larger at $r/r_{1/2} \approx 1$ than at $r/r_{1/2} \approx 0$ and decreases with increasing z/D_j. This trend is consistent for both reference and modeled results. However, the mean $\mathcal{P}_r^{SGS}$ tends to be overestimated by a factor between 2 and 5 with respect to the filtered values. The spread of the reference and modeled $\mathcal{P}_r$ PDFs is qualitatively similar (except for the negative part). Nonetheless,

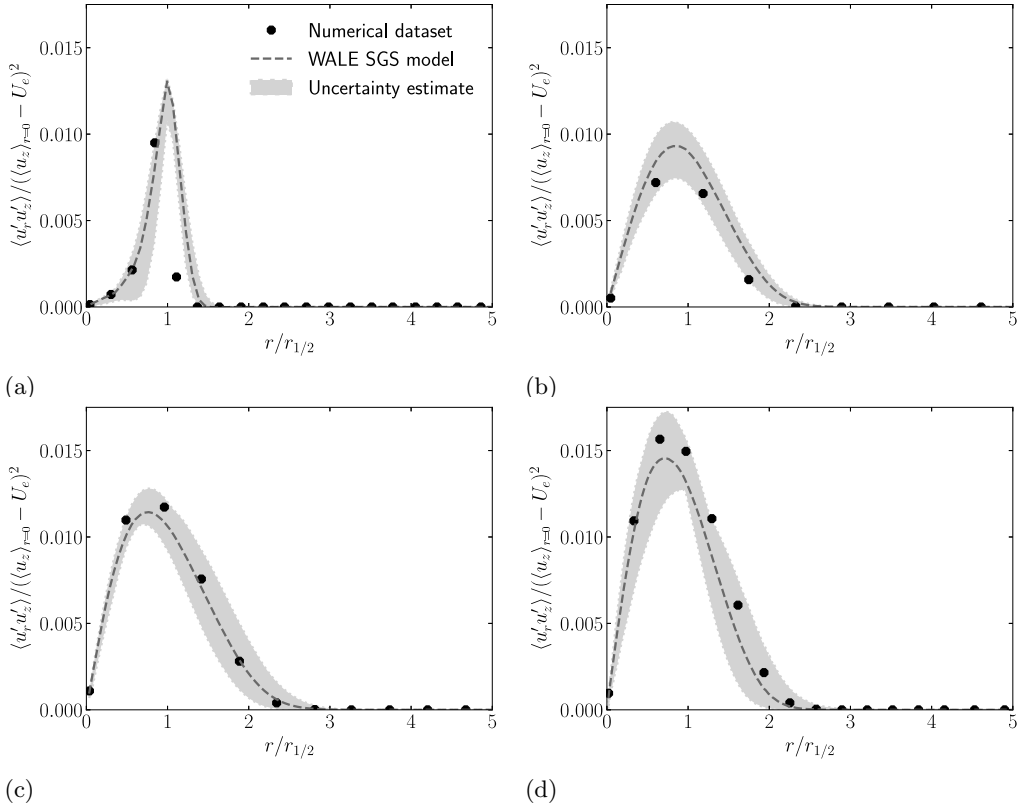

FIGURE 8. Comparison of WALE SGS uncertainty estimates against the numerical dataset. Radial profiles of Reynolds shear stress at different axial positions: (a) $z/D_j \approx 1$, (b) $z/D_j \approx 5$, (c) $z/D_j \approx 10$, (d) $z/D_j \approx 20$.

the overall discrepancy in terms of $\mathcal{P}_r$ is not exceedingly large for the flow studied in this work. This is not typically the case in multiphysics flow problems in which small-scale phenomena impose significant misalignment between τ_{ij} and $\overline{S}_{ij}$, such as in combustion flames and two-phase interfaces.

4. Sensitivity analysis of model-form uncertainties

The model-form uncertainty estimation framework developed also enables researchers to perform systematic sensitivity studies. Based on the discrepancies analyzed in Section 3, the impact of magnitude and shape model-form uncertainties on the QoIs are examined. These two uncertainties consider three of the six degrees of freedom of τ_{ij} and are independently related to $\mathcal{P}_r$ through the factor $2\nu_{SGS}$ in the case of eddy-viscosity-type closures (magnitude) and the sum of $\lambda_i - \gamma_i$ products (anisotropy). Upon selection of the WALE SGS closure as the base model, propagation of incertitude in the magnitude of τ_{ij}^{SGS} is studied by augmenting and decreasing τ_{kk} as proposed by the maximum and minimum limits of the perturbation framework. Model-form uncertainty in the spectrum of τ_{ij}^{SGS} is analyzed by perturbing the eigenvalues of the base model tensor toward the three vertices of the barycentric map with relative distances $\Delta_B = 5\%$. The shaded regions in Figures 5-9 depict the envelope of predictions resulting from the perturbation

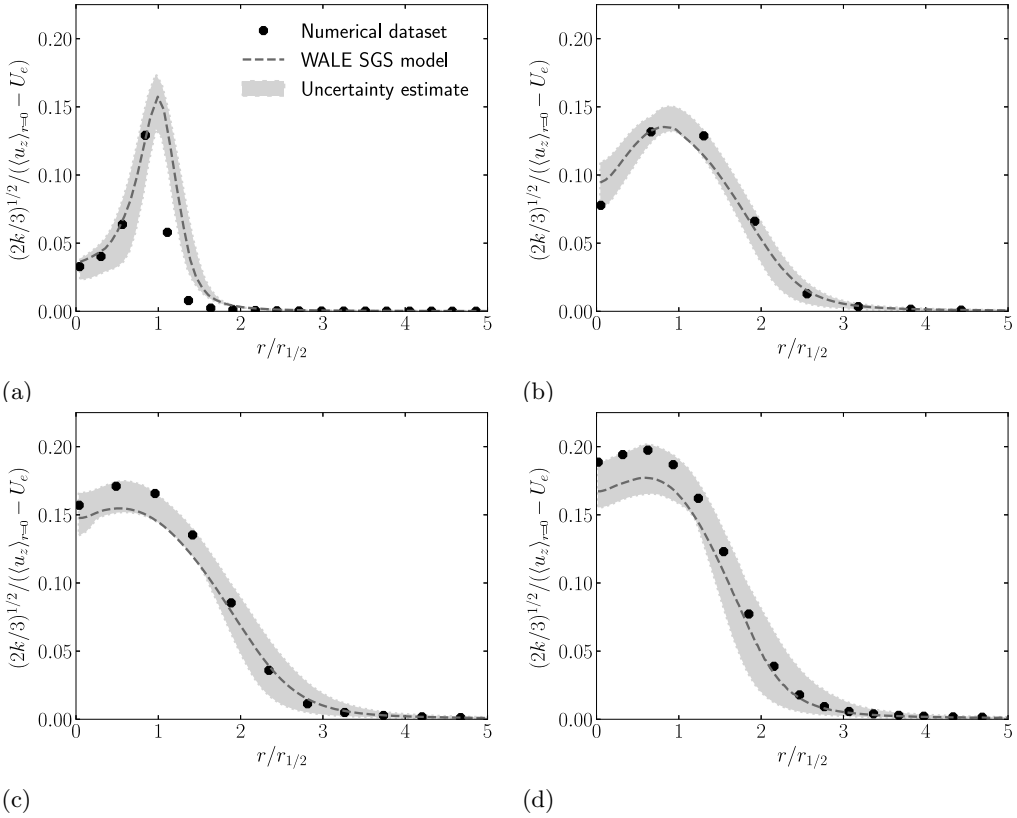

FIGURE 9. Comparison of WALE SGS uncertainty estimates against the numerical dataset. Radial profiles of turbulent kinetic energy at different axial positions: (a) $z/D_j \approx 1$, (b) $z/D_j \approx 5$, (c) $z/D_j \approx 10$, (d) $z/D_j \approx 20$.

UQ estimation. In general, the uncertainty estimates adaptively envelope the reference data for most of the profiles, displaying wider regions at points where the base model significantly deviates from the reference solution.

Results of uncertainty estimates for mean axial velocity profiles are depicted in Figure 5. The shaded regions, representative of the uncertainty perturbation solutions, clearly envelope the reference data along the jet axis and radial profiles at different axial positions. Moreover, the width of the envelopes broadens in regions where discrepancy between the WALE model and reference data predictions increases, i.e., $z/D_j > 5$ and $r/r_{1/2} < 2$, whereas it narrows away from the axis where the turbulence activity is lower. For these plots, the upper and lower bounds correspond to the solutions obtained by reducing the trace of the tensor and by perturbing the eigenvalues toward vertex $\mathbf{x}_{1c}$ of the barycentric map, respectively. The performance of the perturbation UQ framework, in terms of enveloping the reference data, is similar for the normal and shear stresses, and the aggregate turbulent kinetic energy, shown in Figures 6-9, except for $z/D_j \approx 1$, in which the numerical dataset is not covered by the space of perturbed solutions for $1 < r/r_{1/2} < 2$. In this region, the flow field is dominated largely by the large scales, with the SGS model not playing an important role. A common observation for the uncertainty estimates of the second-order statistics is that the width of the shaded areas slightly increases with z/D_j. In addition, the bounds of the envelopes display a general

change of trend: the upper and lower bounds for $r/r_{1/2} < 1$ result from augmenting the trace and forcing the SGS stresses to be more rod-like, while perturbing toward a rod-like shape and reducing the magnitude provide the upper and lower bounds for $r/r_{1/2} > 1$. In general, the first- and second-order QoIs studied are sensitive to reducing the magnitude and increasing the anisotropy of τ_{ij}^{SGS} in one direction. On the contrary, they are strongly independent to the other perturbations considered: increase of tensor magnitude and anisotropy perturbation toward two- and three-component vertices.

5. Conclusions

An eigenspace-based sensitivity analysis of SGS model-form uncertainty has been performed on a LES of a circular turbulent jet. Experimental and numerical reference data have been utilized to validate the observations of the study in terms of averaged and rms axial and radial velocities, shear stresses and turbulent kinetic energy. The numerical reference dataset has been generated by means of carrying out highly accurate (DNS-like resolution) simulations based on the setup of the reference experiment. Focus has been placed on QoIs at the jet's centerline and half-width for different axial distances, as these correspond to regions of the flow characterizing the potential core and exhibiting maximum production of turbulent kinetic energy, respectively. Complete agreement between the reference datasets has been obtained for first- and (virtually) second-order flow statistics.

Differences in statistics between the numerical reference solution and a LES based on the eddy-viscosity WALE SGS model have been observed for the averaged axial velocity along the jet axis in the interaction region and, more significantly, for second-order flow quantities in $r/r_{1/2} < 1$. *A-priori* eigendecomposition analyses of differences between reference and modeled SGS stress tensors have shown that the correlation between tensors in terms of anisotropy is outstandingly low, as the reference tensor tends to lie close to the one-component vertex and two-component limit of the barycentric map while the PDF of the modeled tensor is concentrated in the central region and axisymmetric contraction limit. In addition, large differences in backscatter between reference and modeled SGS kinetic energy production due to the shape and orientation of the SGS stresses imposed in the construction of the WALE model have been identified.

On the basis of the *a-priori* discrepancy observations, the impact of magnitude and anisotropy model-form uncertainty on different QoIs have been *a-posteriori* analyzed. The general observation is that the uncertainty estimates adaptively envelope the reference data, displaying wider regions at points where the base model significantly deviates from the reference solution. The reduction of SGS stresses' magnitude and perturbation toward one-component anisotropy provide the larger impacts on flow statistics. Perturbations to the shape of the tensor present, in general, larger relative impact than reducing, or augmenting, the magnitude of the tensor; similar order deviations are observed for both types of discrepancies, but the perturbations related to shape discrepancy are relatively small (5%) compared with the $\mathcal{O}(1)$ magnitude perturbations. A common observation for the uncertainty estimates is that the width of the envelopes slightly increases with axial distance, indicating that model-form uncertainty is characterized by a cumulative behaviour in free shear flows.

Acknowledgments

This investigation was funded by the Advanced Simulation and Computing (ASC) program of the US Department of Energy's National Nuclear Security Administration via the PSAAP-II Center at Stanford University (Grant No. DE-NA0002373). Sandia National Laboratories is a multi-mission laboratory managed and operated by National Technology and Engineering Solutions of Sandia, LLC., a wholly owned subsidiary of Honeywell International, Inc., for the U.S. Department of Energy's National Nuclear Security Administration under contract DE-NA0003525. This paper describes objective technical results and analysis. Any subjective views or opinions that might be expressed in the paper do not necessarily represent the views of the U.S. Department of Energy or the United States Government (SAND2018-13232B).

REFERENCES

Amielh, M., Djeridane, T., Anselmet, F. & Fulachier, L. 1996 Velocity near-field of variable density turbulent jets. *Int. J. Heat Mass Transfer* **39**, 2149–2164.

Banerjee, S., Krahl, R., Durst, F. & Zenger, C. 2007 Presentation of anisotropy properties of turbulence, invariants versus eigenvalues approaches. *J. Turbul.* **8**, 1–27.

Cantwell, B. J. 2002 *Introduction to Symmetry Analysis*. Cambridge University Press.

Chapman, D. & Kuhn, G. 1986 The limiting behavior of turbulence near a wall. *J. Fluid Mech.* **170**, 265–292.

Cheung, S., Oliver, T., Prudencion, E., Pridhomme, S. & Moser, R. 2011 Bayesian uncertainty analysis with applications to turbulence modeling. *Reliab. Eng. Syst. Safe* **96**, 1137–1149.

Clark, R. A., Ferziger, J. H. & Reynolds, W. C. 1979 Evaluation of subgrid-scale models using an accurately simulated turbulent flow. *J. Fluid Mech.* **91**, 1–16.

Domino, S. P. 2015 Sierra Low Mach Module: Nalu Theory Manual 1.0. *Tech. Rep.* SAND2015-3107W. Sandia National Laboratories, Unclassified Unlimited Release (UUR).

Dunn, M. C., Shotorban, B. & Frendi, A. 2011 Uncertainty quantification of turbulence model coefficients via Latin hypercube sampling method. *J. Fluids Eng.* **133**, 041402.

Emory, M., Larsson, J. & Iaccarino, G. 2013 Modeling of structural uncertainties in Reynolds-averaged Navier-Stokes closures. *Phys. Fluids* **25**, 110822.

Germano, M. 1992 Turbulence: the filtering approach. *J. Fluid Mech.* **238**, 325–336.

Germano, M., Piomelli, U., Moin, P. & Cabot, W. 1991 A dynamic subgrid-scale eddy viscosity model. *Phys. Fluids A* **3**, 1760–1765.

Ghosal, S. 1996 An analysis of numerical errors in large-eddy simulations of turbulence. *J. Comput. Phys.* **125**, 187–206.

Gorlé, C. & Iaccarino, G. 2013 A framework for epistemic uncertainty quantification of turbulent scalar flux models for Reynolds-averaged Navier-Stokes simulations. *Phys. Fluids* **25**, 055105.

Iaccarino, G., Mishra, A. A. & Ghili, S. 2017 Eigenspace perturbations for uncertainty estimation of single-point turbulence closures. *Phys. Rev. Fluids* **2**, 024605.

Jofre, L., Domino, S. P. & Iaccarino, G. 2018 A framework for characterizing structural uncertainty in large-eddy simulation closures. *Flow Turbul. Combust.* **100**, 341–363.

Kim, J. & Choi, H. 2009 Large eddy simulation of a circular jet: effect of inflow conditions on the near field. *J. Fluid Mech.* **620**, 383–411.

Kuerten, J. G. M. 2016 Point-particle DNS and LES of particle-laden turbulent flow — a state-of-the-art review. *Flow Turbul. Combust.* **97**, 689–713.

Lucor, D., Meyers, J. & Sagaut, P. 2007 Sensitivity analysis of large-eddy simulations to subgrid-scale-model parametric uncertainty using polynomial chaos. *J. Fluid Mech.* **585**, 255–280.

Meldi, M., Lucor, D. & Sagaut, P. 2011 Is the Smagorinsky coefficient sensitive to uncertainty in the form of the energy spectrum? *Phys. Fluids* **23**, 125109.

Meyers, J., Geurts, B. J. & Baelmans, M. 2003 Database analysis of errors in large-eddy simulation. *Phys. Fluids* **15**, 2740.

Meyers, J. & Sagaut, P. 2007*a* Evaluation of Smagorinsky variants in large-eddy simulations of wall-resolved plane channel flows. *Phys. Fluids* **19**, 095105.

Meyers, J. & Sagaut, P. 2007*b* Is plane-channel flow a friendly case for the testing of large-eddy simulation subgrid-scale models? *Phys. Fluids* **19**, 048105.

Nicoud, F. & Ducros, F. 1999 Subgrid-scale stress modelling based on the square of the velocity gradient. *Flow Turbul. Combust.* **62**, 183–200.

Olsson, M. & Fuchs, L. 1996 Large eddy simulation of the proximal region of a spatially developing circular jet. *Phys. Fluids* **8**, 2125.

Parish, E. J. & Duraisamy, K. 2016 A paradigm for data-driven predictive modeling using field inversion and machine learning. *J. Comput. Phys.* **305**, 758–774.

Phillips, N. A. 1970 Models for weather prediction. *Annu. Rev. Fluid Mech.* **2**, 251–292.

Pitsch, H. 2006 Large-eddy simulation of turbulent combustion. *Annu. Rev. Fluid Mech.* **38**, 453–482.

Pope, S. B. 2000 *Turbulent Flows*. Cambridge University Press.

Safta, C., Blaylock, M., Templeton, J., Domino, S., Sargsyan, K. & Njam, H. 2017 Uncertainty quantification in LES of channel flow. *Int. J. Numer. Meth. Fluids* **83**, 376–401.

Sagaut, P. & Grohens, R. 1999 Discrete filters for large eddy simulation. *Int. J. Numer. Meth. Fluids* **31**, 1195–1220.

Smagorinsky, J. 1963 General circulation experiments with the primitive equations. I. The basic experiment. *Mon. Weather Rev.* **91**, 99–164.

Stevens, B., Moeng, C.-H., Ackerman, A. S., Bretherton, C. S., Chlond, A., de Roode, S., Edwards, J., Golaz, J.-C., Jiang, H., Khairoutdinov, M., Kirkpatrick, M.P., Lewellen, D.C., Lock, A., Muller, F., Stevens, D.E., Whelan, E. & Zhu, P. 2005 Evaluation of large-eddy simulations via observations of nocturnal marine stratocumulus. *Mon. Weather Rev.* **133**, 1443–1462.

Völker, S., Moser, R. & Venugopal, P. 2002 Optimal large eddy simulation of turbulent channel flow based on direct numerical simulation statistical data. *Phys. Fluids* **14**, 3675–3691.

Wang, P., Frohlich, J., Michelassi, V. & Rodi, W. 2008 Large-eddy simulation of variable-density turbulent axisymmetric jets. *Int. J. Heat Fluid Flow* **29**, 654–664.

Xiao, H., Wu, J.-L., Wang, J.-X., Sun, R. & Roy, C.J. 2016 Quantifying and reducing model-form uncertainties in Reynolds-averaged Navier-Stokes simulations: a data-driven, physics-informed Bayesian approach. *J. Comput. Phys.* **324**, 115–136.